

Design monolayer iodinenes based on halogen bond and tiling theoryKejun Yu ^{1,2}, Yichen Liu,^{1,2} Botao Fu,³ Run-Wu Zhang,^{1,2} Da-shuai Ma,^{4,5} Xiao-ping Li,⁶ Zhi-Ming Yu ^{1,2,*},
Cheng-Cheng Liu ^{1,2,†} and Yugui Yao^{1,2}¹*Centre for Quantum Physics, Key Laboratory of Advanced Optoelectronic Quantum Architecture and Measurement (MOE),
School of Physics, Beijing Institute of Technology, Beijing 100081, China*²*Beijing Key Lab of Nanophotonics and Ultrafine Optoelectronic Systems, School of Physics,
Beijing Institute of Technology, Beijing 100081, China*³*College of Physics and Electronic Engineering, Center for Computational Sciences,
Sichuan Normal University, Chengdu 610068, China*⁴*Institute for Structure and Function and Department of Physics and Chongqing Key Laboratory for Strongly Coupled Physics,
Chongqing University, Chongqing 400044, People's Republic of China*⁵*Center of Quantum Materials and Devices, Chongqing University, Chongqing 400044, People's Republic of China*⁶*School of Physical Science and Technology, Inner Mongolia University, Hohhot 010021, China*

(Received 20 October 2023; revised 6 February 2024; accepted 22 February 2024; published 20 March 2024)

Xenes, two-dimensional (2D) monolayers composed of a single element, with graphene as a typical representative, have attracted widespread attention. Most of the previous Xenes, X from group-III A to group-VI A elements, have bonding characteristics of covalent bonds. In this paper, we unveil the pivotal role of a halogen bond, which is a distinctive type of bonding with interaction strength between that of a covalent bond and a van der Waals interaction, in 2D group-VII A monolayers. Combining the ingenious non-edge-to-edge tiling theory and state-of-the-art *ab initio* method with refined local density functional M06-L, we provide a precise and effective bottom-up construction of 2D iodine monolayer sheets, iodinenes, primarily governed by halogen bonds, and successfully design a category of stable iodinenes encompassing herringbone, Pythagorean, gyrate-truncated hexagonal, i.e., diatomic kagome, and gyrate hexagonal tiling patterns. These iodine structures exhibit a wealth of properties, such as nontrivial topology, flat bands and fascinating optical characteristics, offering valuable insights and guidance for future experimental investigations. Our paper not only unveils the unexplored halogen bonding mechanism in 2D materials but also opens an avenue for designing other noncovalent bonding 2D materials.

DOI: [10.1103/PhysRevB.109.125423](https://doi.org/10.1103/PhysRevB.109.125423)**I. INTRODUCTION**

Two-dimensional (2D) materials have been a hot topic since the discovery of graphene. Up to now, as one of the most important members of 2D materials, increasing Xenes, with X made from group-III to -VI elements, have been predicted and synthesized, including borophene, silicene, phosphorene, tellurene, and so on [1–11]. Generally, disparate valence electron configurations among diverse main group elements engender markedly distinct structural arrangements, bonding behaviors, and material characteristics within the various Xene families. Yet, as one of the most intriguing members of the Xene family, rare study on group-VII Xenes has been done. Undoubtedly, exploring the theoretical foundations of group-VII Xenes will enhance our understanding of 2D materials and generate a more extensive range of practical applications.

Solid halogen crystals exhibit a layered structure in the $Cmca$ space group [12], with stacked planar monolayers. Among the halogens, only iodine maintains its crystalline phase under ambient conditions. The halogen bond (XB, X

stands for halogen), akin to hydrogen bonds as a noncovalent interaction [13,14], plays a crucial role in stabilizing bulk iodine, despite often being overlooked. Recently, few-layer iodine nanosheets have been experimentally obtained from bulk iodine by physical exfoliation [15–18], but the fine structure of the iodinenes remains unclear. On the other hand, it is noteworthy that XBs have been utilized for fabricating halogen-bonded organic frameworks (XOFs) [19,20] successfully with reliable stability in both solid and solution phases. Then the questions naturally arise: Could 2D iodinenes be constructed by utilizing halogen bonding interactions, how to design them, and what interesting properties do such 2D materials have?

In this paper, based on the XBs, we predict a series of monolayer iodinenes as another category of 2D materials utilizing the tiling theory and first-principles calculations. First, through our meticulous density functional theory (DFT) calculations, including the calculations of lattice parameters and phonon spectra, we find that M06-L [21] is an appropriate exchange-correlation functional for evaluating the XB and realize that the XB plays a key role in the formation of stable structures of halogen crystals. Herringbone iodine, as monolayer iodine exfoliated from bulk iodine, shows dynamic stability resulting from XB

*zhiming_yu@bit.edu.cn

†ccliu@bit.edu.cn

networks. Afterward, according to the interaction model of XB and taking into account the diversity of XB networks, we systematically design a series of structures of iodinenes based on halogen-bonded iodine molecules and the tiling theory to map the structure. Finally, we investigate the electronic structures of our designed iodinenes. All of these halogen-bonded iodinenes are semiconductors and exhibit nontrivial band topology, including herringbone, Pythagorean, gyrated truncated hexagonal (GTH), i.e., diatomic kagome, and gyrated hexagonal (GH) iodinenes. Specifically, herringbone, Pythagorean, GTH/diatomic-kagome, and GH iodinenes are intrinsic Stiefel-Whitney topological insulators with higher-order bulk-edge correspondences, among which Pythagorean, GTH/diatomic-kagome, and GH iodinenes are Z_2 topological insulators exhibiting helical edge states with appropriate filling. These iodinenes possess flat bands that result from XB interactions and special structures, leading to remarkable absorption coefficients that exceed 10^5cm^{-1} in the visible region, which reveals the potential for photoelectronic applications.

II. THE HALOGEN BOND AND SELECTION OF DFT FUNCTIONAL

Figure 1(a) depicts the layered structure of bulk iodine. Specifically, each planar layer within the bulk iodine is formed by halogen-bonded iodine molecules. The electrostatic interaction model offers an intuitive image of XBs, as depicted in Fig. 1(b), which displays the electrostatic potential (ESP) map of a monolayer iodine sheet. The unique ESP map is derived from the inherent anisotropic charge density distribution [see Fig. S1(b)] of the iodine molecules themselves, where the electron density is accumulated around the equator and depleted on the elongation of the covalent bond. The depleted region is the so-called σ hole [22], corresponding to the blue tip in Fig. 1(b) with positive ESP. The XB is defined as the attraction between a nucleophilic region and the positive electrostatic region of a σ hole, analogous to a hydrogen bond [23]. Additionally, weak van der Waals (vdW) forces dominate the interaction between layers along the c axis in the bulk iodine. This arrangement reveals the potential for exfoliation to yield a freestanding monolayer of iodine, given the significantly greater strength of the XB compared to vdW interactions.

A comparative analysis of various GGA and meta-GGA functionals was conducted to evaluate their computational accuracy in modeling the interactions within bulk iodine. The results indicate that M06-L accurately captures the attractive XB interaction in bulk iodine, whereas SCAN [24] does not exhibit this capability (see Fig. S2). This finding is consistent with the study by George *et al.* [25]. It is pertinent to highlight that the utilization of PBE [26] and PBEsol [27] functionals for assessing the interaction associated with halogen bonding is deemed inappropriate (as delineated in Figs. S1 and S2 and Table S1), despite their application in recent research [28]. To account for long-range dispersive interactions, the DFT-D3 method [29] was employed, resulting in a more accurate geometry configuration for bulk iodine (as demonstrated in Table S1). Therefore, M06-L+D3 was chosen for the DFT

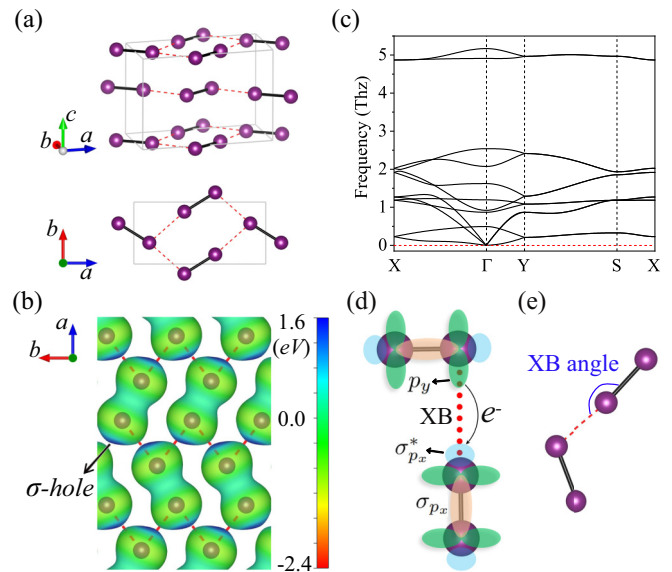


FIG. 1. (a) 3D crystal structure (the upper panel) of bulk iodine and its monolayer (the lower panel). Black bold and red dashed lines indicate intramolecular covalent bonds and intermolecular halogen bonds (XBs), respectively. (b) Electrostatic potential (ESP) map on 0.015 a.u. charge density isosurface of monolayer herringbone iodine. A σ hole occurs at the blue tip on the isosurface with positive electrostatic potential. (c) Phonon spectra of monolayer herringbone iodine. (d) Schematic diagram of XB between two iodine molecules. The iodine atoms, p_y orbitals (lone pairs), σ_{p_x} bond, and $\sigma_{p_x}^*$ antibond orbitals (σ hole) are depicted as purple balls, green spindles, yellow ellipsoid, and blue ellipsoid, respectively. p_z and s orbitals are not shown here because p_z sits out of plane and s is the core orbital. The red dotted line signifies the presence of the XB, involving the transfer of electrons from a lone pair to a σ hole through a donor-acceptor interaction. (e) Schematic diagram of XB angle.

calculations. Further computational details can be found in the Supplemental Material (SM) [30].

III. DESIGN IODINENES WITH THE TILING THEORY

First, a monolayer iodine is exfoliated from bulk iodine, and we call it herringbone iodine since the profile resembles herringbone. After relaxation, the intramolecular bond length and XB length are 2.75 and 3.60 Å, respectively, with only minor deviations from the bulk counterparts. Additionally, the ESP map of the herringbone iodine is similar to that of the monolayer iodine sheet in bulk [see Fig. 1(b)]. There is no imaginary frequency in phonon spectra [Fig. 1(c)] of freestanding monolayer iodine, revealing its dynamic stability. The XB network plays a crucial role in enabling individual iodine molecules to link with each other to form a planar structure, while herringbone iodine would bear dynamic instability if XB is not included (see Fig. S5).

Considering the crucial role of XB in forming stable bulk iodine and an exfoliated monolayer, we now provide a general and effective bottom-up construction of monolayer iodinenes based on XB, with the usage of ingenious non-edge-to-edge tiling theory, to find all the structures as exhaustively as

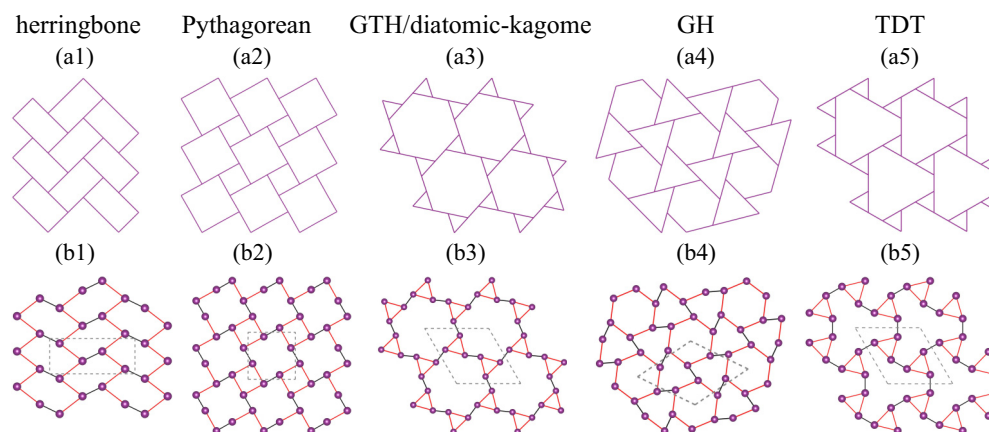


FIG. 2. (a1)–(a5) Five non-edge-to-edge tilings for mapping to desired monolayer iodinenes and (b1)–(b5) corresponding relaxed crystal structures. The nomenclature of those tilings is adopted in a visualized way. Herringbone: herringbone tiling; GTH: gyrated truncated hexagonal tiling, which is topologically equivalent to diatomic-kagome structures; GH: gyrated hexagonal tiling; TDT: truncated distorted trihexagonal tiling. In (b1)–(b5), the covalent bond and halogen bond are depicted by black and red lines, respectively. Grey dotted lines indicate the unit cell.

possible. Geometrically, it is evident that herringbone iodine can be achieved by placing iodine atoms at each vertex of a hexagonal herringbone tiling, with the long edges representing the XBs. Therefore, we aim to construct iodinenes by bonding diatomic iodine molecules with XBs and utilizing the tiling theory [31–33].

The molecular orbital picture of the halogen bonding between two iodine molecules provides a valuable reference for constructing the halogen bonding network under investigation. As shown in Fig. 1(d), each molecule has one σ_{p_x} bond, two p_y orbitals (lone pairs), and one $\sigma_{p_x}^*$ antibond orbital [34]. The s orbital forms a core pair and the p_z orbital lies out of plane, so they are ignored in the formation of XB. Electrons on the top diiodine could be transferred from the p_y lone pair to the $\sigma_{p_x}^*$ antibond orbital on the bottom diiodine, which is the orbital interaction picture of halogen bonding [35]. For the case of herringbone iodine, every molecule acts as both an electron donor and acceptor, constituting an XB net [red dashed line in Fig. 1(b)]. Hence, from the XB interaction picture in herringbone iodine, several essential points can be derived to guide the construction of iodine. (1) Each diiodine molecule exhibits two σ holes and two lone pairs within the same plane, enabling each atom to form two connections with other diiodines. Constructing monolayer iodine based on the XB network is equivalent to a one-to-one correspondence between the σ hole and the lone pair. (2) Iodine is expected to be planar, as all σ holes and lone pairs involved in the XB are confined to the same plane. (3) Every iodine atom should be considered equivalent to one another, in principle. There is no justification for discrimination among them, as the XBs occur uniformly between diiodine molecules.

The tiling theory can help us construct iodinenes systematically. If any two polygons are either disjoint or share one vertex or one entire edge in common, tiling by convex polygons is called edge-to-edge tiling [36,37]. In contrast, if adjacent tiles share only part of their edge, this is the so-called non-edge-to-edge tiling. Some works have predicted structures of 2D covalent materials utilizing the tiling theory [31–33], more specifically, within the edge-to-edge

classification. Regarding iodinenes, there are refined concepts that involve non-edge-to-edge tilings. First, each atom is treated as a vertex, and intramolecular bonds and XBs are represented as edges in the tiling. Second, each vertex is connected to three edges, two of which have equal lengths, which corresponds to the case that each iodine atom connects a covalent bond and two equidistant XBs. Additionally, adjacent edges with equal lengths cannot be collinear because the σ hole and p_y lone pair on the same atom cannot be in alignment. Lastly, all vertices should be equivalent, meaning they are related by the symmetry of the tiling, known as vertex-transitive or uniform tiling [36,37]. Based on this analysis, we can identify the required tilings from the existing non-edge-to-edge patterns [38]. The results are presented in Fig. 2.

Five non-edge-to-edge tilings [see Figs. 2(a1)–2(a5)] are selected from the existing 91 types of uniform tiling [38] to map the tiling pattern to iodine structure. Hence, the nomenclatures of those iodinenes could be labeled by their tiling patterns. The initial length of the short and long edges are set as 2.75 and 3.60 Å, respectively, according to the intramolecular and XB length in the case of monolayer herringbone iodine, and all XB angles [see sketch map at Fig. 1(e)] are set as 180°. After structural relaxation, all the initial structures are slightly distorted. Bonding features could be seen from the charge density and ESP map (Figs. S6 and S7). The herringbone pattern [Fig. 2(b1)] is the same as the foregoing herringbone iodine. The Pythagorean tiling [Fig. 2(a2)] is tessellated by two different sized squares, whose name originates from the *Pythagorean* theorem, so we call the corresponding structure Pythagorean iodine [Fig. 2(b2)]. GTH [see Fig. 2(a3)] is composed of regular hexagons and regular trigons, resembling the diatomic-kagome lattice topologically. As for the GH tiling see Fig. 2(a4), XB forms the entire edge of the hexagon and partial edge of the trigon, which is reversed from the case of GTH. The fifth pattern is truncated distorted trihexagonal tiling (TDT) [see Fig. 2(a5)], which is composed of small regular trigons and big distorted truncated trigons. More details such as the symmetry and Wyckoff position of these iodinenes are shown in Table S2. The phonon

spectra are calculated (see Fig. S10), revealing that herringbone, Pythagorean, GH, and GTH/diatomic-kagome iodinenes exhibit no imaginary frequency.

To comprehensively explore the potential structures of monolayer iodinenes, we employed additional conventional methods to generate more 2D configurations. (a) We assume some simple lattices, including square, triangle, honeycomb, lieb, kagome, etc. (see Fig. S21). These iodinenes behave as conventional covalent 2D crystals where iodine serves as a polyvalent element and are highly energetic and dynamically unstable (see Fig. S23), part of which is even more energetic than gas diiodine that is not likely to form a stable freestanding crystal (see Table S2). (b) We manually connect diiodine-based building blocks (see Fig. S8) solely through XBs, without employing the knowledge of the tiling theory. Nine configurations (see Fig. S9) are obtained, and two of them (T4 and T4+T4m, as detailed in the SM [30]) didn't appear before. However, both T4 and T4+T4m exhibit dynamic instability (Fig. S10). This result may be attributed to the violation of the requirement for all iodine atoms to be equivalent. (c) Additionally, a structure search using the particle swarm optimization (PSO) method [39] is conducted (see Fig. S21). The PSO search identifies the emergence of herringbone and Pythagorean iodinenes in our design. However, several low-energy configurations, such as GTH and GH iodinenes, are not detected. The contrast highlights the distinct effectiveness of our design.

Formation energy (ΔE , meV/molecule) of all configurations derived is listed in Table S2, with the energy of gas diiodine being the reference zero, where both M06-L+D3 and PBE functionals are used. Under the M06-L+D3 scheme, herringbone is the most low-energetic iodine structure ($\Delta E = -509$), followed by Pythagorean ($\Delta E = -457$), T4+T4m, TDT, GH, T4, and GTH. These seven configurations consist of halogen-bonded iodine molecules and possess the lowest energy exactly. Conversely, high-energetic configurations are comprised of iodine molecules without XB nets, like ITSS (isosceles triangle snub square) and OR (octagon rhombus), or manifest as covalent crystals (refer to Fig. S22). These outcomes collectively demonstrate the genuine inclination of monolayer iodinenes toward arrangements formed through halogen-bonded iodine molecules, thereby substantiating the value and validity of our devised approach.

The thermodynamic stability of herringbone, Pythagorean, GH, and GTH iodinenes are checked by performing the *ab initio* Born-Oppenheimer molecular dynamics (AIMD) simulations at 300 K, 200 K, and 100 K in the NVT ensemble [40]. Herringbone and Pythagorean iodinenes perfectly maintain their framework at 200 K. In comparison, GH and GTH iodinenes do at 100 K. Therefore, all the four iodinenes can be observed at a temperature higher than the liquid nitrogen.

IV. BAND TOPOLOGY IN MONOLAYER IODINENES

We find herringbone, Pythagorean, GTH/diatomic-kagome, and GH iodinenes are higher-order topological insulators. Due to both inversion symmetry and time-reversal symmetry being preserved in these four configurations, their higher-order topology can be characterized by the second Stiefel-Whitney number w_2 [41]. Here, two methods are

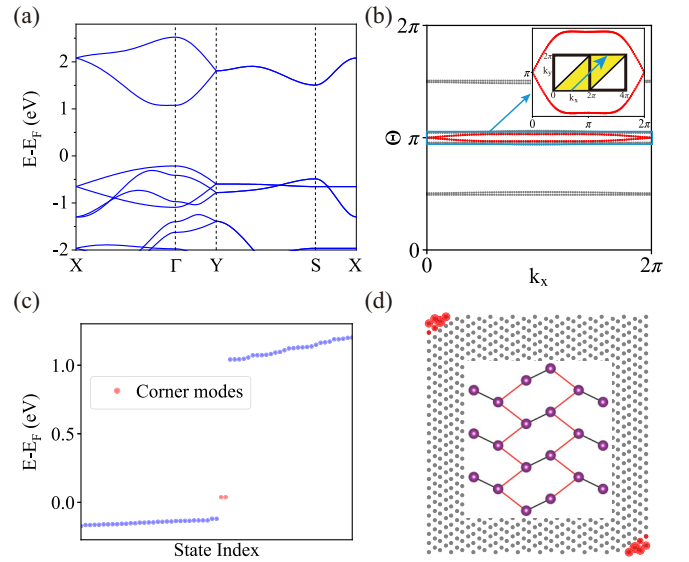


FIG. 3. (a) Band structures of monolayer herringbone iodine. (b) The Wilson loop along k_{110} direction. Insets represent the enlarged Wilson loop around $\Theta = \pi$, indicating the nontrivial higher-order topology with the nonzero second Stiefel-Whitney number. (c) Energy spectra in real space, with the energy of the two corner states highlighted in red. (d) The distribution of the two corner states (depicted in red) in real space.

taken into consideration to prove their higher-order band topology: the parity criterion and the Wilson loop method. For the parity criterion, w_2 can be calculated by the parity eigenvalues of the valence bands,

$$(-1)^{w_2} = \prod_{i=1}^4 (-1)^{\lfloor N_{\text{occ}}^-(\Gamma_i)/2 \rfloor}, \quad (1)$$

where Γ_i are the four time-reversal invariant momenta (TRIMs), N_{occ}^- denotes the number of valence bands with odd parity and $\lfloor \dots \rfloor$ is the floor function. Taking herringbone iodine as an example, we find that $N_{\text{occ}}^-(\Gamma_i)$ are 6, 8, 7, and 7 for Γ , M , X , and Y , respectively, leading to a nontrivial second Stiefel-Whitney number $w_2 = 1$. This indicates that the herringbone iodine is a higher-order topological insulator. The nontrivial w_2 can also be evidenced by the Wilson loop method. In Fig. 3(b), we plot the Wilson loop of the herringbone iodine along the k_{110} direction. One can find that the Wilson loop has only one crossing point on $\Theta = \pi$. This again proves the higher-order topology of the herringbone iodine. Therefore, the herringbone iodine would have 0D-protected corner states. This is confirmed by our numerical calculation. The numerical result is plotted in Fig. 3(c), from which two corner states in the band gap can be clearly observed. The charge density distributions of corner states in real space are presented in Fig. 3(d). The other three kinds of iodinenes are also calculated as second Stiefel-Whitney insulators with nontrivial w_2 (see Figs. S12–S14 and Table S3).

Spin-orbit coupling (SOC) induced band topology is also studied considering the iodine element possesses a non-negligible SOC strength. As for the cases of Pythagorean, GTH/diatomic-kagome, and GH iodinenes, band crossings between the highest valence band and its lower band are all opened by SOC, which induces band inversions (see

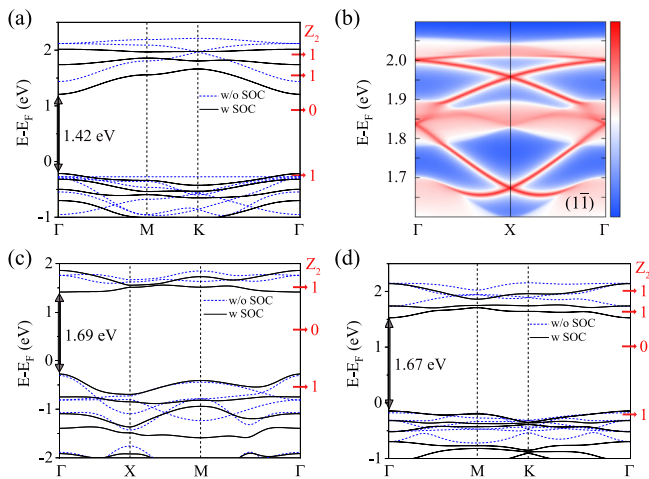


FIG. 4. (a) Band structures of GTH/diatomic-kagome iodinene. (b) Helical edge states of GTH/diatomic-kagome iodinene along the $(1\bar{1})$ edge. (c), (d) Band structures of Pythagorean and GH iodinenes respectively. Blue dashed lines and black lines are the band structures without and with spin-orbit coupling (SOC) respectively. Grey arrows indicate the band gap. Topological Z_2 invariants are labeled above the occupied states defined.

Fig. 4). And the same behavior occurs between the lowest conduction band and its upper band. For spatial inversion invariant systems [42], we can calculate the topological Z_2 invariant by counting the parity of the occupied states and find that these iodinenes are 2D topological insulators if the Fermi energy is shifted above the lowest unoccupied band or below highest occupied band. As shown in Fig. 4(b), the gapless helical edge states connect the bulk states of GTH/diatomic-kagome iodinene, corresponding to the Z_2 values labeled in Fig. 4(a), which originates from the bulk-boundary correspondence. Considering 2D materials are fabricated generally on substrates, the Fermi level could be shifted by choosing an appropriate substrate or doping. Hence these iodinenes could serve as a potential topological insulator.

V. FLAT BANDS AND OPTICAL ABSORPTION

As a noncovalent bond, XB could result in flat-band structures in iodinenes because the relatively weak interactions between iodine molecules, and the flat band would bring about some unique properties. The band structures of herringbone iodinene are depicted in Fig. S19(a), where a quasidirect band gap (1.165 eV) emerges between the conduction band minima (CBM) at Γ and valence band maxima (VBM) near Γ . Notably, the highest occupied band from Γ to VBM is almost flat with an energy shift of about only 8 meV (31 meV for HSE06), so it is a direct gap semiconductor approximately. The in-plane absorption coefficient curve is presented in Fig. 5(a), with two distinct peaks (around 2.04 and 2.74 eV) exceeding $3 \times 10^5 \text{ cm}^{-1}$ in the visible region. This value is considerably higher than that observed in many other 2D materials and organic perovskite materials ($10^4 \sim 10^5 \text{ cm}^{-1}$ [43]). As a result, herringbone iodinene is promising for the photoelectric conversion of solar energy.

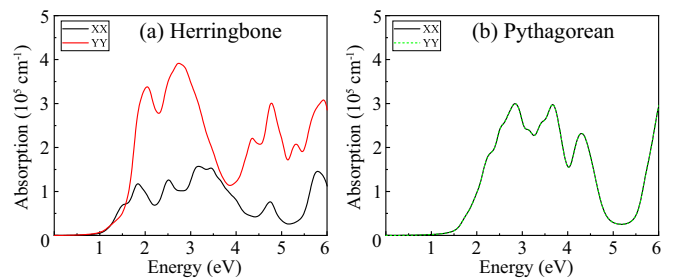


FIG. 5. Computed in-plane optical absorption coefficients of (a) herringbone and (b) Pythagorean iodinenes in a unit of 10^5 cm^{-1} as a function of photon energy. XX and YY indicate the directions along two primitive vectors of unit cell.

As shown in Fig. 4, Pythagorean, GTH, and GH iodinenes are direct-gap semiconductors with the gap being 1.69, 1.42, and 1.67 eV, respectively. Notably, GTH iodinene possesses a diatomic-kagome lattice leading to two flat bands [44,45] around -0.27 and 2.12 eV without SOC and one flat band around 2.0 eV with SOC. If with an appropriate substrate or heterojunction, the flat band is promising for a strong correlation platform. In addition, the computed in-plane optical absorption coefficients for Pythagorean, GTH, and GH iodinenes all exceed 10^5 cm^{-1} within the visible range (with peaks between $2 \sim 3$ eV, see Figs. 5(b) and S20). These flat bands resulting from XBs and geometry contribute to the high density of states and are beneficial to strong optical absorption, indicating their potential applications in photoelectronic devices.

VI. CONCLUSION AND DISCUSSION

An innovative approach to the design of monolayer iodinenes has been put forward, involving the mapping of unique non-edge-to-edge tilings onto iodinene structures that consist of halogen-bonded iodine molecules. The effectiveness of this method has been validated through first-principles calculations, including the identification of four dynamically stable structures: herringbone, Pythagorean, GTH/diatomic-kagome, and GH. These iodinenes are confirmed as higher-order topological insulators with distinguishable corner states. And flat bands emerge, causing exceptional optical absorption within the visible light range. Furthermore, these iodinenes exhibit direct or quasidirect band gaps, holding potential for optoelectronic applications. Moreover, Pythagorean, GTH/diatomic-kagome, and GH iodinenes showcase non-trivial Z_2 band topology with appropriate doping. Notably, traditional approaches, including PSO searching, yield many structures devoid of halogen bonds. Those structures exhibit dynamic instability and higher energies than iodinenes formed by halogen-bonded iodine molecules. This outcome underscores the preference for iodinenes constructed from halogen-bonded iodine molecules, further substantiating the rationality of our design approach and bringing about a unique vision for the structural composition of 2D materials.

Different from other Xenas as covalent crystals, iodinene belongs to a category of 2D crystals where XBs dominate.

As XBs have extensive applications in crystal engineering [46,47], catalysis [48], supramolecular chemistry [49,50], biomolecular systems [51], self-assembly [52,53], and drug design [54], etc. already, monolayer iodinenes including herringbone, Pythagorean, GTH/diatomic-kagome and GH patterns would provide another platform to explore more innovations.

Note added. Recently, we became aware of an independent work [55]. The work also studies the 2D sheet of iodine.

ACKNOWLEDGMENTS

We thank J. Cao, C. Cui, X. Zhou, X. Yang, and L. Liu for their helpful discussions. The paper is supported by the National Key R&D Program of China (Grant No. 2020YFA0308800), the National Natural Science Foundation of China (Grants No. 12374055 and No. 12204330), and the Science Fund for Creative Research Groups of NSFC (Grant No. 12321004).

-
- [1] A. J. Mannix, X.-F. Zhou, B. Kiraly, J. D. Wood, D. Alducin, B. D. Myers, X. Liu, B. L. Fisher, U. Santiago, J. R. Guest, M. J. Yacaman, A. Ponce, A. R. Oganov, M. C. Hersam, and N. P. Guisinger, *Science* **350**, 1513 (2015).
- [2] X. Wu, J. Dai, Y. Zhao, Z. Zhuo, J. Yang, and X. C. Zeng, *ACS Nano* **6**, 7443 (2012).
- [3] B. Aufray, A. Kara, S. Vizzini, H. Oughaddou, C. Léandri, B. Ealet, and G. Le Lay, *Appl. Phys. Lett.* **96**, 183102 (2010).
- [4] C.-C. Liu, W. Feng, and Y. Yao, *Phys. Rev. Lett.* **107**, 076802 (2011).
- [5] K. Takeda and K. Shiraishi, *Phys. Rev. B* **50**, 14916 (1994).
- [6] H. Liu, A. T. Neal, Z. Zhu, Z. Luo, X. Xu, D. Tománek, and P. D. Ye, *ACS Nano* **8**, 4033 (2014).
- [7] L. Li, Y. Yu, G. J. Ye, Q. Ge, X. Ou, H. Wu, D. Feng, X. H. Chen, and Y. Zhang, *Nat. Nanotechnol.* **9**, 372 (2014).
- [8] Z. Zhu, X. Cai, S. Yi, J. Chen, Y. Dai, C. Niu, Z. Guo, M. Xie, F. Liu, J.-H. Cho, Y. Jia, and Z. Zhang, *Phys. Rev. Lett.* **119**, 106101 (2017).
- [9] M. Zhou, W. Ming, Z. Liu, Z. Wang, P. Li, and F. Liu, *Proc. Natl. Acad. Sci. USA* **111**, 14378 (2014).
- [10] H. Zhao, C.-w. Zhang, W.-x. Ji, R.-w. Zhang, S.-s. Li, S.-s. Yan, B.-m. Zhang, P. Li, and P.-j. Wang, *Sci. Rep.* **6**, 20152 (2016).
- [11] F. Reis, G. Li, L. Dudy, M. Bauernfeind, S. Glass, W. Hanke, R. Thomale, J. Schäfer, and R. Claessen, *Science* **357**, 287 (2017).
- [12] F. van Bolhuis, P. B. Koster, and T. Michelsen, *Acta Crystallogr.* **23**, 90 (1967).
- [13] P. Brunet, M. Simard, and J. D. Wuest, *J. Am. Chem. Soc.* **119**, 2737 (1997).
- [14] R.-B. Lin, Y. He, P. Li, H. Wang, W. Zhou, and B. Chen, *Chem. Soc. Rev.* **48**, 1362 (2019).
- [15] M. Qian, Z. Xu, Z. Wang, B. Wei, H. Wang, S. Hu, L.-M. Liu, and L. Guo, *Adv. Mater.* **32**, 2004835 (2020).
- [16] C. Kuang, W. Zeng, M. Qian, and X. Liu, *ChemPlusChem* **86**, 865 (2021).
- [17] Y. You, Y.-X. Zhu, J. Jiang, Z. Chen, C. Wu, Z. Zhang, H. Lin, and J. Shi, *J. Am. Chem. Soc.* **145**, 13249 (2023).
- [18] Y. Ye, Y. Wang, K. Zhang, W. Guo, T. Kong, X. Ding, N. Zhao, and F. Xu, *Biomater. Sci.* **11**, 1311 (2023).
- [19] G. Gong, S. Lv, J. Han, F. Xie, Q. Li, N. Xia, W. Zeng, Y. Chen, L. Wang, J. Wang *et al.*, *Angew. Chem.* **133**, 14957 (2021).
- [20] N. Chongboriboon, K. Samakun, T. Inprasit, F. Kielar, W. Dungkaew, L. W.-Y. Wong, H. H.-Y. Sung, D. B. Ninkovi, S. D. Zari, and K. Chainok, *CrystEngComm* **22**, 24 (2020).
- [21] Y. Zhao and D. G. Truhlar, *J. Chem. Phys.* **125**, 194101 (2006).
- [22] T. Clark, M. Hennemann, J. S. Murray, and P. Politzer, *J. Mol. Model.* **13**, 291 (2007).
- [23] G. R. Desiraju, P. S. Ho, L. Kloo, A. C. Legon, R. Marquardt, P. Metrangolo, P. Politzer, G. Resnati, and K. Rissanen, *Pure Appl. Chem.* **85**, 1711 (2013).
- [24] J. Sun, A. Ruzsinszky, and J. P. Perdew, *Phys. Rev. Lett.* **115**, 036402 (2015).
- [25] J. George, C. Reimann, V. L. Deringer, T. Bredow, and R. Dronskowski, *ChemPhysChem* **16**, 728 (2015).
- [26] J. P. Perdew, K. Burke, and M. Ernzerhof, *Phys. Rev. Lett.* **77**, 3865 (1996).
- [27] J. P. Perdew, A. Ruzsinszky, G. I. Csonka, O. A. Vydrov, G. E. Scuseria, L. A. Constantin, X. Zhou, and K. Burke, *Phys. Rev. Lett.* **100**, 136406 (2008).
- [28] A. W. Huran, H.-C. Wang, A. San-Miguel, and M. A. L. Marques, *J. Phys. Chem. Lett.* **12**, 4972 (2021).
- [29] S. Grimme, J. Antony, S. Ehrlich, and H. Krieg, *J. Chem. Phys.* **132**, 154104 (2010).
- [30] See Supplemental Material at <http://link.aps.org/supplemental/10.1103/PhysRevB.109.125423> for (a) computational details; (b) construct monolayer iodinenes from non-edge-to-edge tilings and building blocks; (c) stability of 2D monolayer iodinenes; (d) electronic structure of herringbone, Pythagorean, GTH/diatomic-kagome, and GH iodinenes; and (e) results of iodinenes from the routine structure search method, which includes Refs. [12,56–64].
- [31] C. Lu, Y. Li, L.-M. Wang, H.-J. Yan, L. Chen, and D. Wang, *Chem. Commun.* **55**, 1326 (2019).
- [32] J. Guan, Z. Zhu, and D. Tománek, *ACS Nano* **8**, 12763 (2014).
- [33] Y. Jin, Y. Hu, and W. Zhang, *Nat. Rev. Chem.* **1**, 0056 (2017).
- [34] A. Y. Rogachev and R. Hoffmann, *J. Am. Chem. Soc.* **135**, 3262 (2013).
- [35] G. Cavallo, P. Metrangolo, R. Milani, T. Pilati, A. Priimagi, G. Resnati, and G. Terraneo, *Chem. Rev.* **116**, 2478 (2016).
- [36] B. Grünbaum and G. C. Shephard, *Math. Mag.* **50**, 227 (1977).
- [37] D. Chavey, in *Symmetry 2*, International Series in Modern Applied Mathematics and Computer Science, edited by I. Hargitta (Pergamon, Amsterdam, 1989), pp. 147–165.
- [38] B. Grünbaum and G. C. Shephard, *Trans. Am. Math. Soc.* **242**, 335 (1978).
- [39] Y. Wang, J. Lv, L. Zhu, and Y. Ma, *Comput. Phys. Commun.* **183**, 2063 (2012).
- [40] G. J. Martyna, M. L. Klein, and M. Tuckerman, *J. Chem. Phys.* **97**, 2635 (1992).
- [41] J. Ahn, D. Kim, Y. Kim, and B.-J. Yang, *Phys. Rev. Lett.* **121**, 106403 (2018).
- [42] L. Fu and C. L. Kane, *Phys. Rev. B* **76**, 045302 (2007).

- [43] X. Huang, Q. Cao, M. Wan, and H.-Z. Song, *Materials* **15**, 6214 (2022).
- [44] G. Sethi, Y. Zhou, L. Zhu, L. Yang, and F. Liu, *Phys. Rev. Lett.* **126**, 196403 (2021).
- [45] H. Liu, S. Meng, and F. Liu, *Phys. Rev. Mater.* **5**, 084203 (2021).
- [46] J. Teyssandier, K. S. Mali, and S. De Feyter, *ChemistryOpen* **9**, 225 (2020).
- [47] P. Metrangolo, G. Resnati, T. Pilati, and S. Biella, in *Halogen Bonding*, Structure and Bonding, Vol. 126, edited by P. Metrangolo and G. Resnati (Springer, Berlin, Heidelberg, 2007), pp. 105–136.
- [48] R. L. Sutar and S. M. Huber, *ACS Catal.* **9**, 9622 (2019).
- [49] A. Priimagi, G. Cavallo, P. Metrangolo, and G. Resnati, *Acc. Chem. Res.* **46**, 2686 (2013).
- [50] P. Metrangolo and G. Resnati, *Chem. Eur. J.* **7**, 2511 (2001).
- [51] P. Auffinger, F. A. Hays, E. Westhof, and P. S. Ho, *Proc. Natl. Acad. Sci. USA* **101**, 16789 (2004).
- [52] E. Corradi, S. V. Meille, M. T. Messina, P. Metrangolo, and G. Resnati, *Angew. Chem., Int. Ed.* **39**, 1782 (2000).
- [53] B. Zha, M. Dong, X. Miao, K. Miao, Y. Hu, Y. Wu, L. Xu, and W. Deng, *J. Phys. Chem. Lett.* **7**, 3164 (2016).
- [54] Y. Lu, T. Shi, Y. Wang, H. Yang, X. Yan, X. Luo, H. Jiang, and W. Zhu, *J. Med. Chem.* **52**, 2854 (2009).
- [55] Z. Zhu, J. Gu, J. Gao, W. Chen, C. Niu, P. Cui, Y. Jia, and Z. Zhang, *Phys. Rev. B* **108**, 115409 (2023).
- [56] G. Kresse, J. Furthmüller, and J. Hafner, *Phys. Rev. B* **50**, 13181 (1994).
- [57] P. E. Blöchl, *Phys. Rev. B* **50**, 17953 (1994).
- [58] G. Kresse and D. Joubert, *Phys. Rev. B* **59**, 1758 (1999).
- [59] A. Togo and I. Tanaka, *Scr. Mater.* **108**, 1 (2015).
- [60] A. A. Mostofi, J. R. Yates, G. Pizzi, Y.-S. Lee, I. Souza, D. Vanderbilt, and N. Marzari, *Comput. Phys. Commun.* **185**, 2309 (2014).
- [61] Q. Wu, S. Zhang, H.-F. Song, M. Troyer, and A. A. Soluyanov, *Comput. Phys. Commun.* **224**, 405 (2018).
- [62] J. Tao, J. P. Perdew, V. N. Staroverov, and G. E. Scuseria, *Phys. Rev. Lett.* **91**, 146401 (2003).
- [63] C. Petrillo, O. Moze, and R. Ibberson, *Phys. B: Condens. Matter* **180-181**, 639 (1992).
- [64] X. Li and F. Liu, *arXiv:2307.11890*.